Improved reconstruction methodology of clinical electron energy spectra based on Tikhonov regularization and generalized simulated annealing

J. H. Wilches-Visbal[a]* • P. Nicolucci[b]

[a]*Faculty of Health Sciences, University of Magdalena, Santa Marta, Colombia*
[b]*Department of Physics, University of Sao Paulo, Ribeirao Preto, Brazil*

Abstract: Electron beam radiotherapy is the most widespread treatment modality to deal with superficial cancers. In electron radiotherapy, the energy spectrum is important for electron beam modelling and accurate dose calculation. Since the percentage depth-dose (PDD) is a function of the beam's energy, the reconstruction of the spectrum from the depth-dose curve represents an inverse problem. Thus, the energy spectrum can be related to the depth-dose by means of an appropriate mathematical model as the Fredholm equation of the first kind. Since the Fredholm equation of the first kind is ill-posed, some regularization method must be used to achieve a useful solution. In this work the Tikhonov regularization function was solved by the generalized simulated annealing optimization method. The accuracy of the reconstruction was verified by the gamma index passing rate criterion applied to the simulated PDD curves for the reconstructed spectra compared to experimental PDD curves. Results show a good coincidence between the experimental and simulated depth-dose curves according to the gamma passing rate better than 95% for 1% dose difference (DD)/1 mm distance to agreement (DTA) criteria. Moreover, the results show improvement from previous works not only in accuracy but also in calculation time. In general, the proposed method can help in the accuracy of dosimetry procedures, treatment planning and quality control in radiotherapy.

*Corresponding author.
E-mail address: jhwilchev@gmail.com(J. H. Wilches-Visbal).

1. Introduction

Electron beam radiotherapy is the most widespread and currently treatment modality utilized to treat superficial cancers. The relatively uniform build-up dose followed by the rapid dose falloff as the beam penetrates deeper into the target justify its clinical usage (Funk et al., 2016; Toutaoui et al., 2009).

In electron therapy, the energy spectrum and bremsstrahlung dose are important clinical characteristics of electron beam modelling (Deasy et al., 1996; Ding & Rogers, 1995) as the beam is composed by a mixture of primary and secondary electrons and photons produced in the internal structures of the medical accelerator (Faddegon & Blevis, 2000; Zhu et al., 2001).

The knowledge of the energy spectrum is critical characteristic when the purpose is accurate dose calculation since it affects the dose distribution (Chvetsov & Sandison, 2002; Faddegon & Blevis, 2000). Furthermore, the energy spectrum may also be relevant in dosimetry (Renner et al., 2014), treatment planning (Deasy et al., 1996), realistic simulations of the beam (de la Vega et al., 2008; Renner et al., 2014) and other clinical problems.

Radiation source modelling by Monte Carlo (Rogers et al., 1995), experimental measurement by means of a magnetic spectrometer (Deasy et al., 1996; Renner et al., 2014) and inverse reconstruction are the most commonly approaches to obtain the energy spectrum of an electron beam (Chvetsov & Sandison, 2002; Zhengming & Jette, 1999).

Inverse reconstruction employs an appropriate mathematical model to extract the spectrum from its dept-dose curve. Advantages of inverse reconstruction over the other approaches include not being necessary to have detailed knowledge about the geometry and composition of the accelerator head; no necessity of building the accelerator head's phase space file, it is computationally fast and only demands depth-dose data which are easily measured in any radiotherapy center (Wilches-Visbal & Da Costa, 2019b). Limitations of inverse reconstruction are related to the determining of the bremsstrahlung dose, the solution of the ill-conditioning of the mathematical model (Chvetsov & Sandison, 2002; Wei et al., 2006) and the accuracy of off-axis dose data.

Since the percentage depth-dose curve (PDD) strongly depends on the electron spectrum, much information about the spectrum is already contained in it (Zhengming & Jette,1999). Fredholm integral equation is used to mathematical linking the centralaxis depth-dose curve to the incident energy spectrum through a kernel function of monoenergetic depth-dose curves (Faddegon & Blevis, 2000; Hansen, 1992; Zhengming & Jette, 1999). As the Fredholm

equation is ill-posed (Hansen, 1992; Kabanikhin, 2008) some regularization method must be used to remove the ill-conditioning of the equation and thereafter getting a useful and stable solution (Golub et al., 1999; Hansen, 2007). Regularization function can be solved by using matrix tools related to singular values decomposition (Hansen, 1992, 2007) or by using an optimization function since the regularization involves a least-square problem (Golub et al., 1999).

In this work, Tikhonov regularization-generalized simulated annealing synergy is employed for obtaining the electron energy spectrum and bremsstrahlung dose at the same optimization process. The depth-dose curves were measured in water for a variety of nominal electron energy beams from a Varian Clinac 21X linear accelerator. Monoenergetic depth-dose curves and simulated depth-dose curves from reconstructed spectra were obtained via PENELOPE 2008 (Salvat et al., 2008) assuming the radiation source is a point source of divergent beam. The gamma index criterion was used to verify the accuracy of this method such as in Wilches-Visbal and Da Costa (2019b).

2. Materials and methods

2.1 Electron Spectrum Unfolding

The unfolding equation regards the electron spectrum incident upon the water phantom surface, $\Phi(E)$, to the experimental depth-dose curve, $D(E)$ (Chvetsov & Sandison, 2002; Faddegon & Blevis, 2000; Zhengming & Jette, 1999),

$$D(z) = \int_{E_{\min}}^{E_{\max}} D_{\mathrm{m}}(z, E)\Phi(E)dE, \qquad (1)$$

where $D_{\mathrm{m}}(z, E)$ is the monoenergetic depth-dose curve from the electron beam of nominal energy E, $E_{\min}$ and $E_{\max}$ are the minimum and maximum energy in the electron beam, respectively.

As clinical electron beams have a certain quantity of photons, some part of $D(z)$ is due to the bremsstrahlung dose. Therefore, Eq. (1) must be modified as,

$$D(z) = \underbrace{\int_{E_{\min}}^{E_{\max}} D_{\mathrm{m}}(z, E)\Phi(E)dE,}_{\text{De:Pure Electron Dose}} + \underbrace{D_c(e^{-\mu_p z} - \vartheta e^{-\mu_e z}),}_{\text{Db: Bremsstrahlung Dose}}$$

$$(2)$$

where D_c is a normalization constant, μ_p is the attenuation coefficient of highenergy photons generated by primary electrons, μ_e is the attenuation coefficient of low-energy photons generated by secondary electrons and $1 - \vartheta$ is a factor related to the surface dose (Brahme & Svensson, 1979).

Eq. (2) can be discretized as,

$$D(z_j) \approx \sum_i D_{\mathrm{m}}(z_j, E_i)\Phi(E_i)\Delta E_i + D_c(e^{-\mu_p z_j} - \vartheta e^{-\mu_e z_j}), \quad (3)$$

where $i \in N$ is the i-th monoenergetic beam with energy E_i, $j \in N$ is the j-th depth of dose measurement bin to the depth and ΔE_i is the energy interval between two consecutive monoenergetic beams.

The Eq. (3) can be represented as a linear equations system,

$$D(z) = K(z,E)\Phi(E) + D_c(e^{-\mu_p z} - \nu e^{-\mu_e z}), \quad (4)$$

where $K = D_m(z,E)\Phi(E)\Delta E$ is a $m \times n$ dimensional matrix known as the kernel function, D is a m-dimensional vector, Φ is a n-dimensional vector and z is a m-dimensional vector.

As Eq. (4) is ill-conditioned (Kabanikhin, 2008), i.e., its solution is extremely sensitive to arbitrarily small perturbations of the system (Hansen, 1992), the calculation of Φ demands applying some regularization method.

Tikhonov regularization, one of the most effective and popular methods for the solution of ill-posed problems (Silva Neto & Cella, 2006; Tikhonov, 1963), filters out the noise in the input data by adding some prior information about the desirable solution (Golub et al., 1999; Hansen, 2007).

In accordance with Hansen (2007), the fundamental idea of Tikhonov regularization is to define the regularized solution Φ_λ as the minimizer of the following weighted combination of the residual norm and the constraint norm

$$\varepsilon_\lambda = \left\| \frac{K\varphi_\lambda}{\max(K\varphi_\lambda)} - \frac{D_z}{\max(D_z)} \right\|_2^2 + \lambda^2 \left\| L\left(\frac{\varphi_\lambda}{\max(\varphi_\lambda)} - \frac{\varphi_0}{\max(\varphi_0)} \right) \right\|_2^2 \quad (5)$$

where λ is the regularization parameter, L is a derivative operator matrix and φ_0 is an a priori information about the energy spectrum to be found (Xu et al., 2016).

To determine the electron energy spectrum, the functional ε_λ in Eq. (5) has to be solved. For this, it is possible to apply techniques of linear algebra such as singular value decomposition (SVD) or generalized singular value decomposition (GSVD) (Hansen, 1992, 2007). Another option to solve the least-square problem involved in Eq. (5) (Golub et al., 1999) is to use an appropriate optimization function or algorithm.

Generalized simulated annealing (GSA) is one the most powerful and widely used optimization algorithms for the solution of global multidimensional functions (Schanze, 2006; Xiang & Gong, 2000). The main idea of GSA is mimicking the annealing, where metal is warmed up to the fusion temperature and immediately after it is cooled sufficiently slowly to achieve a crystalline structure free from imperfections (Wilches-Visbal & Da Costa, 2019a).

GSA function works well in many situations for $q_v = 2.7$, $q_a = -5.0$ and $100 \leq t_{max} \leq 1500$, where q_a, q_v and t_{max} are the acceptance parameter, visiting parameter and maximum iteration number, respectively (Wilches-Visbal & Da

Costa, 2019a). Nonetheless, the choice of q_a, q_v and t_{max} depends on each problem (Xuet al., 2016).

2.2. Reconstruction methodology

The methodology used for obtaining the electron energy spectra and the bremsstrahlung dose curves is summarized as follows:

(I)   Experimental depth-dose curves, $D(z)$, kernel function, $K(z,E)$ and initial energy spectrum, φ_0, are obtained and calculated as in Wilches-Visbal and Da Costa (2019b). In summarize, experimental depth-dose curves are obtained in a clinical setting for different nominal energy beams. The Kernel function is the matrix of monoenergetic depth-dose curves ranged from 0.125 to 19 MeV in 0.125 MeV intervals. The initial spectrum is represented as a Gaussian probability distribution.

(II) Maximum energy of electrons Emax is empirically adjusted as,

$$E_{max} = 2.2R_p + E/10 \quad (6)$$

with, E, the nominal energy of electron beam and, R_p, the practical range (Gerbi et al., 2009). Emax is the cut-off energy of the energy spectrum.

(III) The regularization parameter, λ, and regularization matrix, L, employed are the same of the previous article (Wilches-Visbal & Da Costa, 2019b).

(IV) The bremsstrahlung dose, D_b, is determined by minimizing the Eq. (7) by means of GSA function ($q_v = 2.7, q_a = 2.7$ and $t_{max} = 1000$),

$$\|K\varphi_\lambda + D_b - D\|_2^2, \quad (7)$$

subject to $0 < D_c \leq 0.2$; $0.0379 \leq \mu_p \leq 0.0631$; $0.33 \leq \mu_e \leq 0.91$ and $0.75 \leq \vartheta \leq 1.84$ (Brahme & Svensson, 1979).

(V)   Bremsstrahlung dose is subtracted from the experimental depth-dose curve to obtain the pure electron depth-dose: $D_e = D - D_b$. Energy spectrum, φ, found in this step is ignored because the spectrum presents the oscillations (noise) proper of an ill-posed problem (Wilches et al., 2020). Consequently, it is necessary to use the Tikhonov regularization for achieving a stable solution.

(VI) The regularized energy spectrum, φ_λ, is derived from $De(z)$ by minimizing the functional ε_λ in Eq. (5), subject to $\varphi_\lambda \geq \vec{0}$, through GSA function ($q_v = 2.7, q_a = -5.0$ and $t_{max} = 1000$).

Once the energy spectrum is reconstructed, it is used to obtain the simulated depth-dose curve using the Monte Carlo package PENELOPE-2008 (Salvat et al., 2008, p. 248). The

irradiation setup in the simulations is the same that were used for the monoenergetic depth-dose curves.

To verify the suitability of spectral reconstruction a comparison between the simulated and experimental depth-dose curves is carried out by means of the gamma passing rate criterion (Li et al., 2011). The same analysis is performed with the dose profiles for every energy beam studied. As no manufacturer provides the energy spectra at the phantom surface, the reconstructed spectra would be \estimated spectra" (Baird, 1981).

Gamma index (Γ) is used to measure the coincidence degree of two dose distribution curves from combination of two factors: i) distance to agreement (DTA) is the distance between a point in the reference dose distribution curve (gold-standard) and the nearest point in the calculated dose distribution curve that has the same dose value, and ii) dose-difference (DD) is the difference between the calculated dose at each point to reference dose at that point (Low et al., 1998).

In 1D, gamma index is depicted in a circle with each axis being the quotient of DTA and DD regarding to its passing criteria as seen in Fig. 1.

According to Fig. 1, Γ is calculated as the euclidean distance of two factors normalized to its respective passing criteria for each point. The minimum value of Γ, γ, is selected and used to evaluate the concordance, such as (OncologyMedPhys, 2019; Low et al., 1998),

$$\Gamma(x,y) = \sqrt{\frac{DTA}{DTA_{\text{passing criterion}}} + \frac{DD}{DD_{\text{passing criterion}}}}, \tag{8}$$

$$\gamma = \min\{\Gamma(x,y)\} \tag{9}$$

In this work, the gamma index passing criterion used to evaluate the suitability of the spectra reconstruction is > 95% with 2%/2mm for depth-dose curves, which is proposed by the American Association of Medical Physics (AAPM) (Chetty et al., 2007). For dose profiles is used a > 95% with 4%/4mm criterion. It is also explored what happens as more stringent criteria are applied to both the depth-dose curves (> 95% with 1%/1mm) and dose profiles (> 95% with 2%/2mm).

Analysis of gamma passing rate is done by using the CalcGamma function described and developed by Geurts (2017). In this paper, the experimental depth-dose curve is used as a reference and the global computation method is used for the gamma index calculations.

3. Results and discussion

Fig. 2 shows the reconstructed energy spectra at the phantom surface of the (a) 6, (b) 9, (c) 12 and (d) 15 MeV electron beams from a Varian Clinac 21EX accelerator.
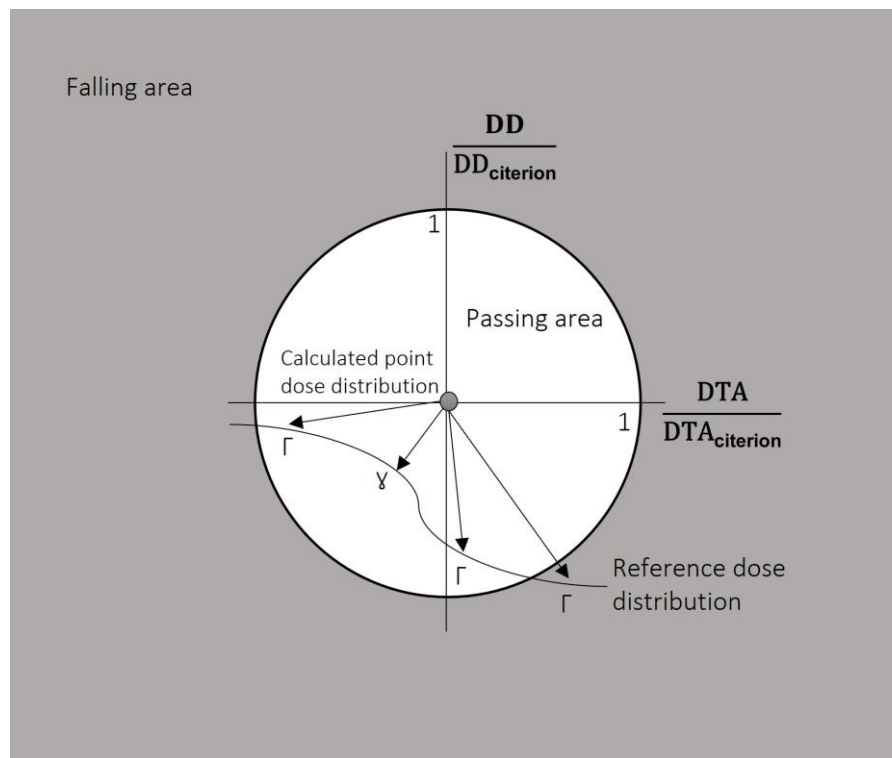

Figure 1. Schematic representation of gamma index. Adapted from (OncologyMedPhys, 2019).
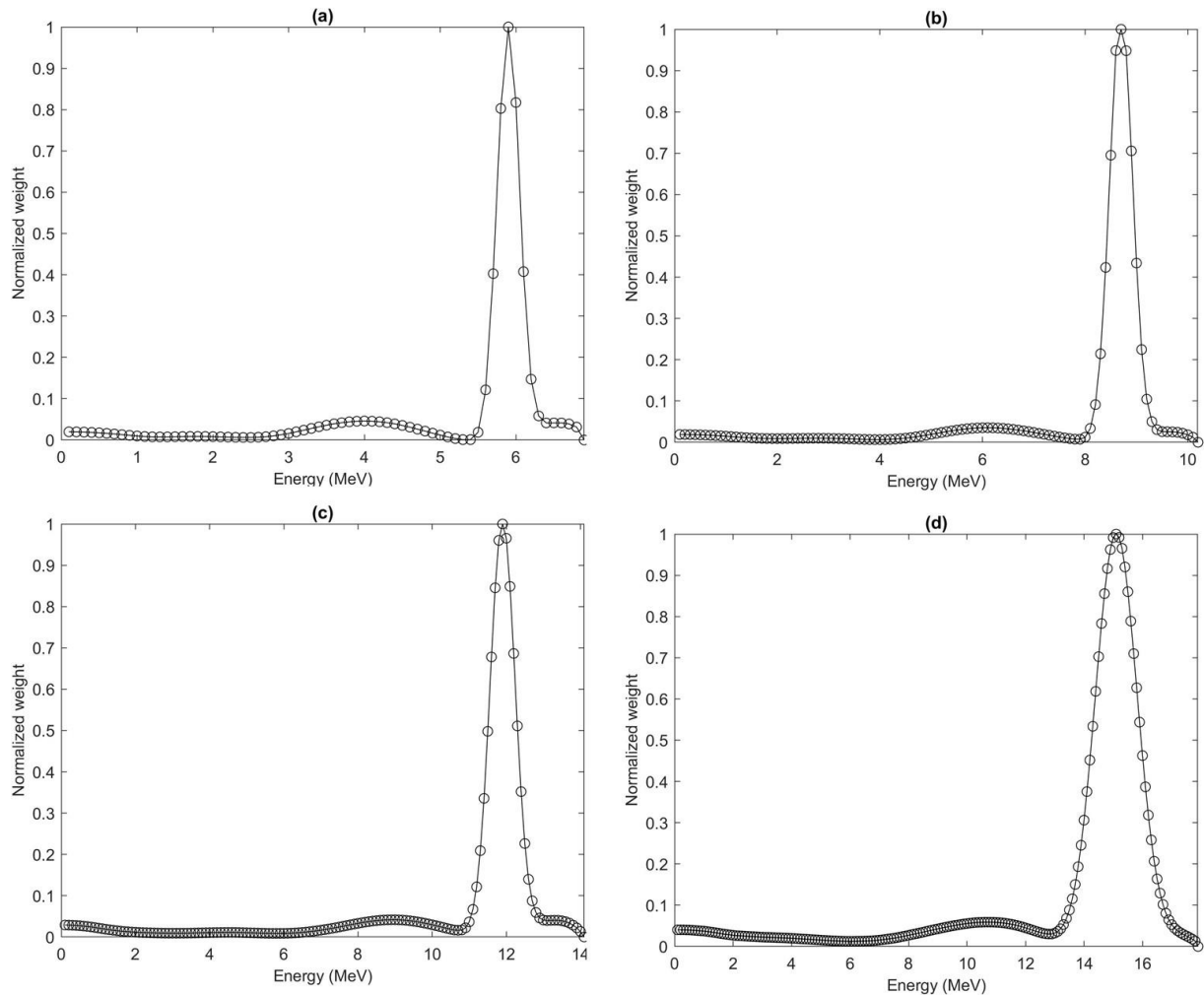
Figure 2. The electron energy spectra at the phantom surface reconstructed by generalized reconstructed simulated annealing for (a) 6 MeV nominal energy, (b) 9 MeV nominal energy, (c) 12 MeV nominal energy and (d) 15 MeV nominal energy. Field size 10x10cm^2 at source skin distance (SSD) of 100 cm.

The most probable energy of the spectra was located at 5.9 MeV for 6 MeV, 8.7 MeV for 9 MeV, 11.9 MeV for 12 MeV and 15.1 MeV for 15 MeV nominal energy beam. The peak width values expressed as $FWHM/E_{mp}$ were 5.8 % for 6 MeV, 6.1 % for 9 MeV, 6.7 % for 12 MeV and 11.1 % for 15 MeV, which indicates a directly proportional relation between peak width and nominal energy of the beam. Values of peak width are slightly lower than those found in Wilches-Visbal and Costa (2019b).

Fig. 3 shows the calculated bremsstrahlung dose by minimizing the Eq. (7) for every clinical electron beam. The x-axis is the depth in the water phantom whilst the y-axis the bremsstrahlung dose relative to the maximum value in the clinical electron depth-dose curve (electrons and photons).

Contrary to Faddegon and Blevis (2000), Deng et al. (2001) and Wilches-Visbal and Da Costa (2019b), the method of linear extrapolation of the bremsstrahlung dose tail or the "Schiff method" has not been used for obtaining the bremsstrahlung dose.

The maximum contribution of bremsstrahlung dose to the experimental depth-dose curve was as much as 3.11% of the maximum dose for 15 MeV, 1.69% for 12 MeV, 0.81% for 9 MeV and 0.39% for 6 MeV nominal energy.

From Fig. 3 can be verified that as nominal energy increases so do the depth of maximum dose, build-up region, and maximum dose value just as it happens in X-ray megavoltage depth-dose curves (Brahme & Svensson, 1979; Deng et al., 2001; Rustgi & Rodgers, 1987).
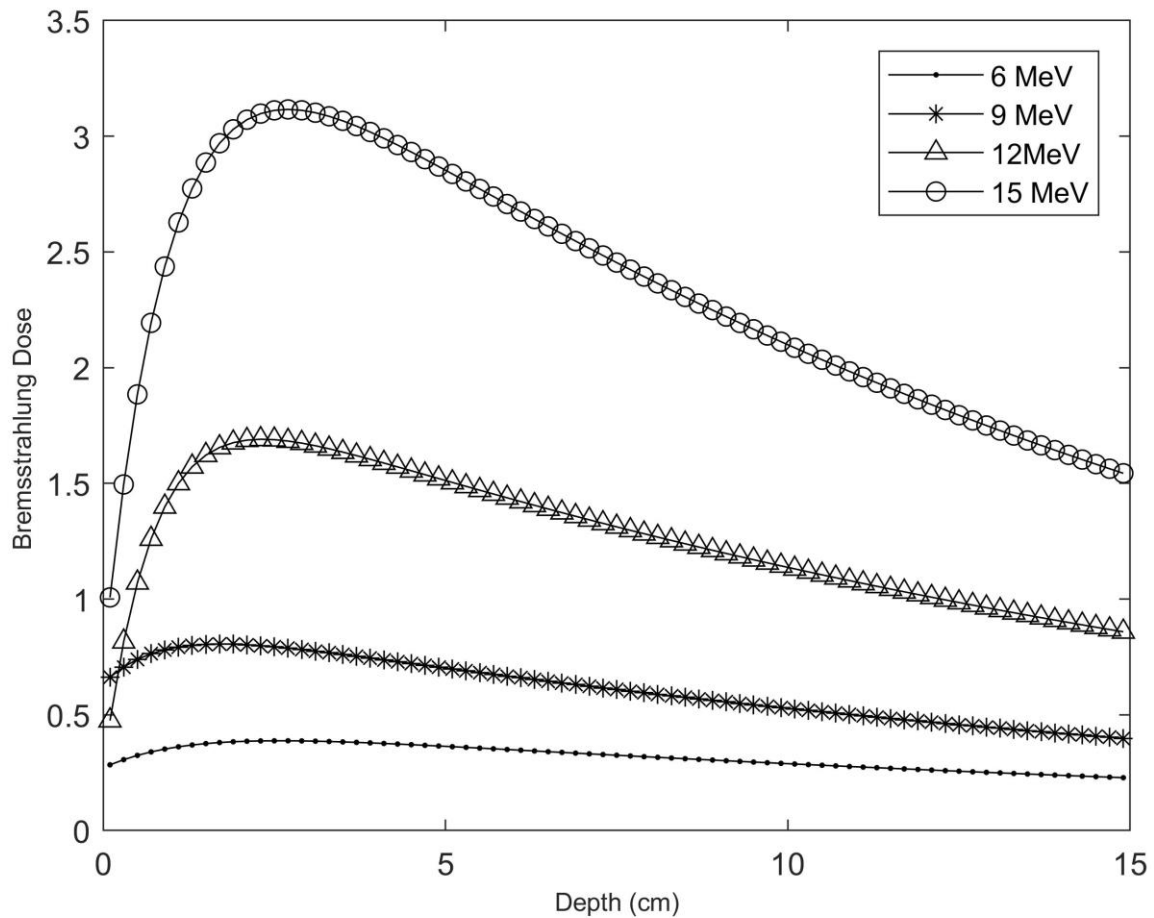
Figure 3. Depth dependence of bremsstrahlung dose relative to the maximum value
in electron depth-dose curve for beams of 6 MeV, 9 MeV, 12 MeV and 15 MeV of
nominal energy. Field size 10x10 cm^2 at SSD of 100 cm.

Some of the important remarks between the bremsstrahlung dose curves calculated by the direct method and the linear-extrapolation one is: i) values of maximum bremsstrahlung dose from the direct method is lower; ii) as depth increases greater differences are found between the values of dose; iii) bremsstrahlung dose calculated from the direct method shows a better agreement to the tail region of the experimental depth-dose curves, just where bremsstrahlung contribution is most relevant.

Indeed, the maximum difference found, given in percentage points (pp), between the experimental and simulated (using the reconstructed spectra) depth-dose curves was 0.14 pp for 6 MeV, 0.16 pp for 9 MeV, 0.16 pp for 12

MeV and 0.22 pp for 15 MeV, which it indicates an optimum agreement in the tail region of PDD curves in Fig. 4. These deviations are less than those found by the extrapolation method (Wilches-Visbal & Da Costa, 2019b), above all for the greater energy electron beams in which the influence of bremsstrahlung dose is most critical (see 15 MeV electron beam in Fig. 4).

In Fig. 4 are displayed the experimental and simulated depth-dose curves for electron beams of nominal energy of (a) 6 MeV, (b) 9 MeV, (c) 12 MeV and (d) 15 MeV. Moreover, it is shown the depth-dose deviation (pp) computed by subtracting the simulated depth-dose from the experimental depth-dose, for every energy beam.
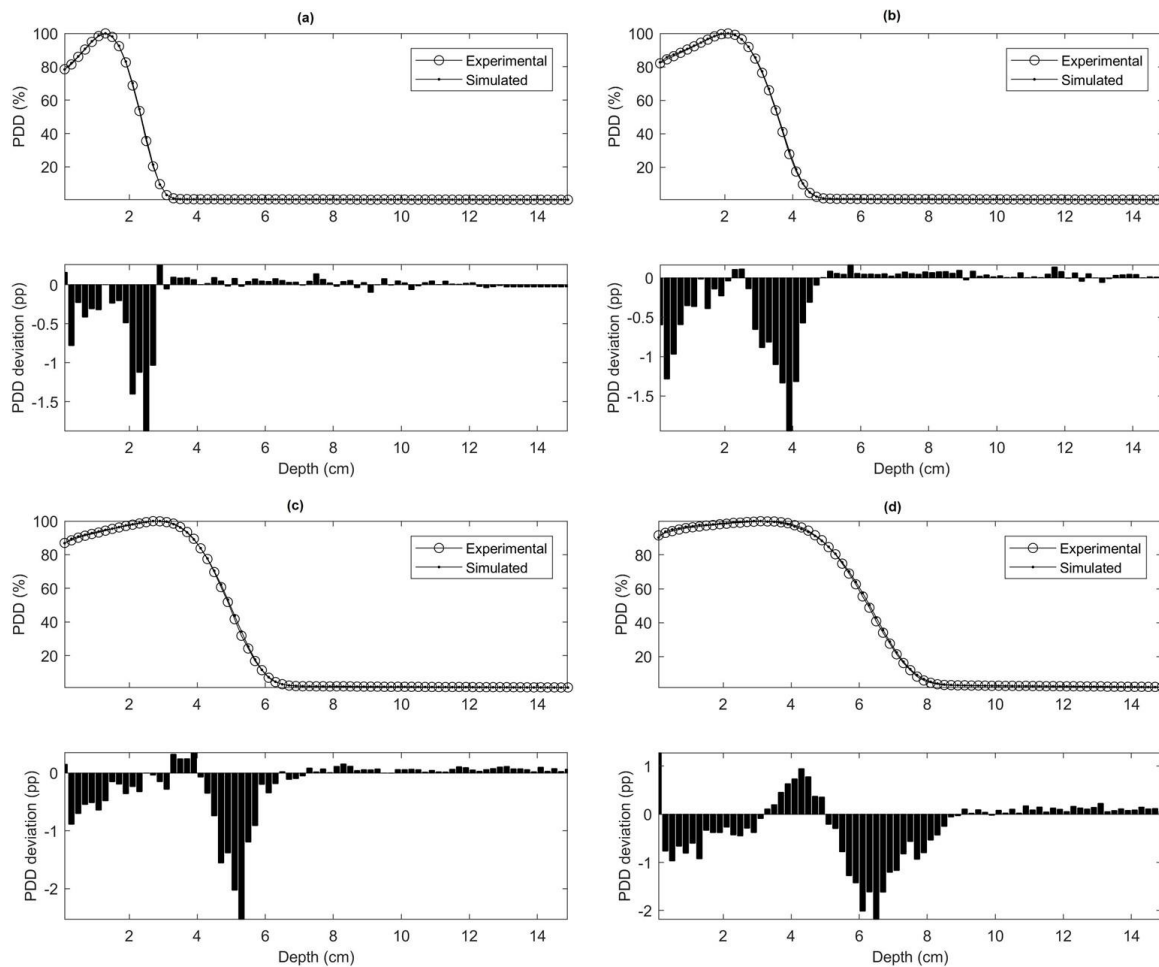
Figure 4. Comparison of simulated (plus-dashed line) and experimental (circle-dot line)
PDD for beams of (a) 6 MeV, (b) 9 MeV, (c) 12 MeV and (d) 15 MeV of nominal energy.
Field size 10x10 cm² at SSD of 100 cm.

In Fig. 4 is shown a reasonable coincidence between the simulated and experimental depth-dose curves in terms of DD for all beams, except for the final part of the fall-off region for the electron beam of 15 MeV where DD ≥ 2%.

Optimum accordance is observed, in terms of DTA, given that no case DTA ≥ 1 mm in any energy electron beam.

Table. 1 shows the gamma passing rate under 2%/2 mm and 1%/1 mm criterion for each electron energy beam.

In Table 1, it is observed that the passing rate is greater than the acceptance threshold established at 95% for all beams. Therefore, it can be said that there are no clinically significant differences between the simulated and experimental depth-dose curves.

On the other hand, comparing these passing rates with the obtained in the early work (Wilches-Visbal & Da Costa, 2019b), these results are better than those, especially for the higher

energy beams. For instance, in this work, the gamma passing rate with 1%/1 mm was 99% while it was 96% in Wilches-Visbal and Da Costa (2019b) for the beam of 15 MeV. Previous papers have reported that discrepancies in the build-up region are due to the angular corrections that have been ignored (Chvetsov & Sandison, 2003; Faddegon & Blevis, 2000).

Nonetheless, it is possible to suppose other reasons such as an improper capture of the low energy components on the algorithm; a choice of low values for the regularization parameters or a poor modelling of the radiation source (point source).

Since the differences in the build-up region found in the early article (Wilches-Visbal & Da Costa, 2019b) are greater than those of the present, it is possible to think that such differences are due to an improper mathematical modelling of the problem. That is, as regularization parameters and

could be the actual reason of the better coincidence in the build-up region as seen in Fig. 4.

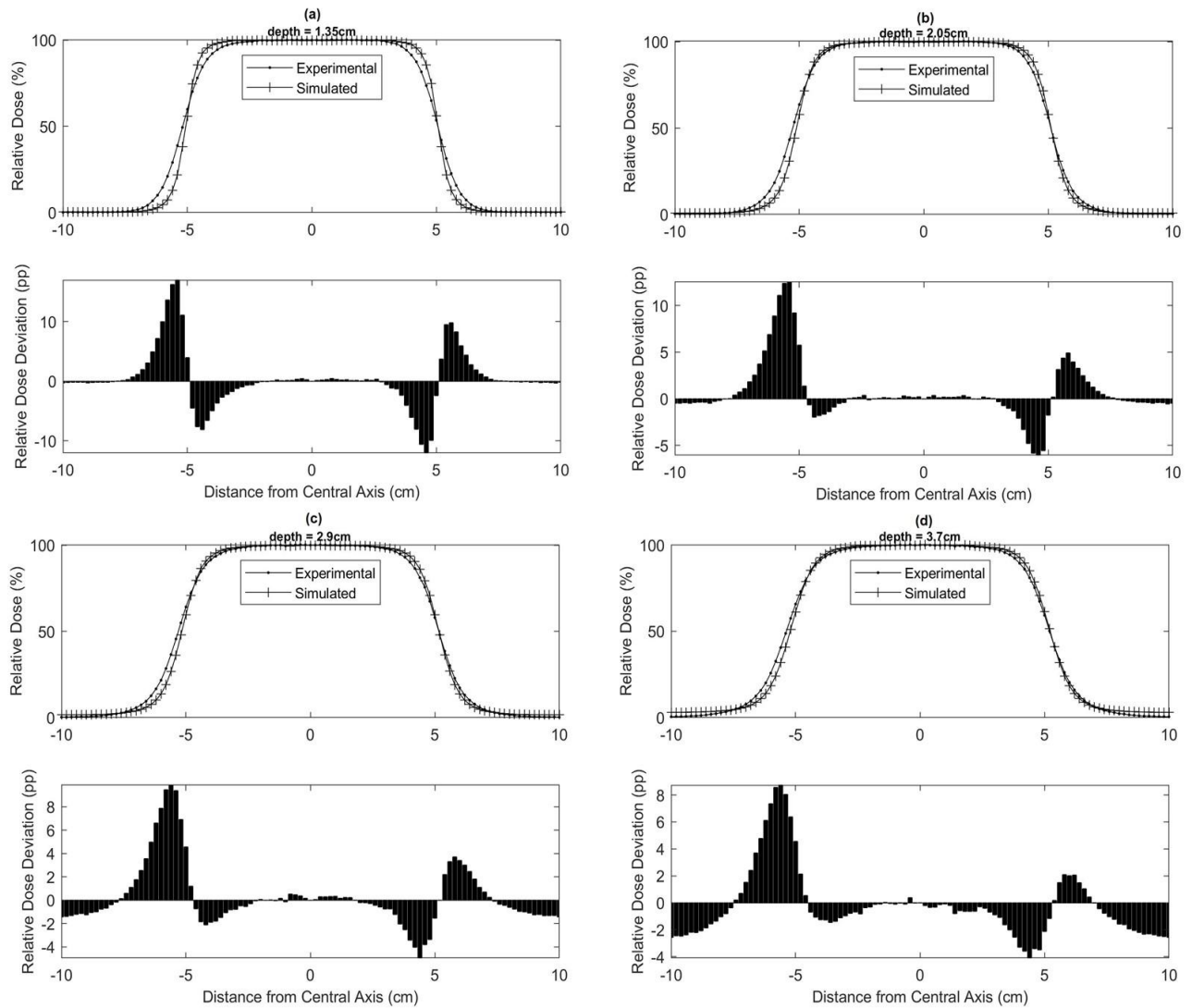In Fig. 5 the dose profiles for all energy beams are depicted.

Figure 5. Comparison of simulated (plus sign line) and the experimental (dotted line) lateral dose profiles at the reference depth for (a) 6 MeV, (b) 9 MeV, (c) 12 MeV and (d) 15 MeV of nominal energy. Field size 10x10 cm² at SSD of 100 cm.

Table 1. Comparison of the simulated and experimental PDD curves by means of the gamma passing rate criterion. For a gamma passing greater than 95% the simulated PDD curves are considered approved.

Nominal Energy (MeV)	Passing Rate (%)	
	2%/2mm	1%/1mm
6	100	100
9	100	100
12	100	100
15	100	99

Dose profiles in Fig. 5 were measured at reference depths of 1.35 cm for 6 MeV, 2.05 cm for 9 MeV, 2.9 cm for 12 MeV and 3.7 cm for 15 MeV electron beam. Furthermore, every dose profile is normalized to the value of dose at the central axis.
Results of the dose profiles gamma passing rate are shown in Table 2.

In Table 2, it is observed that the computed gamma passing rate is greater than the preestablished threshold except for the 6 MeV energy beam such as in Wilches-Visbal and Da Costa (2019b). For a less stringent gamma passing rate (95% with 4%/4 mm) all dose profiles meet the acceptance threshold.

Table 2. Comparison of the simulated dose profiles and experimental dose profiles by means the gamma passing rate criterion at reference depth. For a gamma passing greater than 95% the simulated profiles are considered approved.

Nominal Energy (MeV)	Passing Rate (%)	
	4%/4mm	2%/2mm
6	100	80
9	100	98
12	100	100
15	100	100

Such as in Wilches-Visbal and Da Costa (2019b), as the nominal energy decreases the worse is the match of the experimental and simulated dose profiles. This worsening can obey the angular spread increases as the nominal energy of the beam decreases. So, it seems that angular corrections are mandatory for lower energy spectra. Beyond this, it is remarkable that the reconstructed central-axis energy spectra can reproduce reasonably well the off-axis dose data for the electron beam of higher nominal energy.

The calculation time for reconstruction the energy spectra and bremsstrahlung dose were 30 s, 60 s, 73 s and 85 s for the 6, 9, 12 and 15 MeV electron beams, respectively. For algorithms and calculations, MATLAB®2015a, v.8.5 (Microsoft Windows 7 Ultimate SP1, CPU: 2.30 GHz, RAM: 4Gb) was utilized.

4. Conclusions

A novel methodology for the determination of the electron spectrum and bremsstrahlung dose of clinical linear accelerators have been developed. This methodology consisted of finding the energy spectrum and bremsstrahlung dose at the same optimization process.

Results showed a good agreement between the experimental and simulated depth-dose curves according to > 95% within 1%/1 mm gamma passing rate for all electron beams studied. An acceptable concordance was also observed between the experimental and simulated dose profiles according to > 95% within 1%/1 mm gamma passing rate except to the lowest energy beam.

It was demonstrated that this reconstruction methodology improved the previously published ones in terms of accuracy given that the gamma passing rate scores were closer to 100%. Besides, an appreciable improvement in terms of calculation speed was also observed.

Despite being a reconstructed central-axis electron energy spectra, a reasonable reproduction of off-axis dose data in dose profiles was obtained except for the lowest nominal energy beam. Considering angular corrections for lower energy beams could improve the results in dose profiles.

To determine if the reconstructed spectra are similar to the real ones, it would be necessary to compare them to those obtained by Monte Carlo simulation or experimental measurements (electron spectrometer) or with those supplied by the manufacturer.

Conflict of interest

There is no conflict of interest to declare.

References

Baird, L. C. (1981). X-ray spectra vs attenuation data: A theoretical analysis. *Medical physics*, *8*(3), 319-323. http://doi.org/10.1118/1.594834

Brahme, A., & Svensson, H. (1979). Radiation beam characteristics of a 22 MeV microtron. *Acta radiologica: oncology, radiation, physics, biology*, *18*(3), 244-272. http://doi.org/10.3109/02841867909128212

Chetty, I. J., Curran, B., Cygler, J. E., DeMarco, J. J., Ezzell, G., Faddegon, B. A., … & Siebers, J. V. (2007). AAPM Task Group Report No. 105 Issues associated with clinical implementation of Monte Carlo-based photon and electron external beam treatment planning. *Medical Physics, 34,* 4818-52. http://doi.org/10.1118/1.2795842

Chvetsov, A. V., & Sandison, G. A. (2002). Reconstruction of electron spectra using singular component decomposition. *Medical physics, 29*(4), 578-591. https://doi.org/10.1118/1.1461840

Chvetsov, A. V., & Sandison, G. A. (2003). Angular correction in reconstruction of electron spectra from depth dose distributions. *Medical physics*, *30*(8), 2155-2158. https://doi.org/10.1118/1.1592031

Deasy, J. O., Almond, P. R., & McEllistrem, M. T. (1996). Measured electron energy and angular distributions from clinical accelerators. *Medical physics*, *23*(5), 675-684. https://doi.org/10.1118/1.597817

Deng, J., Jiang, S. B., Pawlicki, T., Li, J., & Ma, C. M. (2001). Derivation of electron and photon energy spectra from electron beam central axis depth dose curves. *Physics in Medicine & Biology*, *46*(5), 1429. https://doi.org/10.1088/0031-9155/46/5/308

de la Vega, J.M., Guirado, D., Vilches, M., Perdices, J. I., & Lallena, A. M. (2008). Obtaining the intrinsic electron spectrum of linear accelerators using the relation between the current of the bending magnet and the absorbed dose in water. *Radiotherapy and Oncology*, *86*(1), 109-113. https://doi.org/10.1016/j.radonc.2007.11.027

Ding, G. X., & Rogers, D. W. O. (1995). Energy spectra, angular spread, and dose distributions of electron beams from various accelerators used in radiotherapy. National Research Council of Canada Report.

Faddegon, B. A., & Blevis, I. (2000). Electron spectra derived from depth dose distributions. *Medical physics*, *27*(3), 514-526. https://doi.org/10.1118/1.598919

Funk, R. K., Stockham, A. L., & Laack, N. N. I. (2016). Basics of Radiation Therapy. *Clinical Cardio-Oncology; Elsevier Inc.: Amsterdam, The Netherlands*, 39-60. https://doi.org/10.1016/b978-0-323-44227-5.00003-x

Gerbi, B. J., Antolak, J. A., Deibel, F. C., Followill, D. S., Herman, M. G., Higgins, P. D., … & Khan, F. M. (2009). Recommendations for clinical electron beam dosimetry: supplement to the recommendations of Task Group 25. *Medical physics*, *36*(7), 3239-3279. https://doi.org/10.1118/1.3125820

Geurts, M. (2017). 1d, 2d or 3d gamma index computation in matlab. Retrieved 22, June 2020 from https://bit.ly/30yW02k

Golub, G. H., Hansen, P. C., & O'Leary, D. P. (1999). Tikhonov regularization and total least squares. *SIAM journal on matrix analysis and applications*, *21*(1), 185–194. https://doi.org/10.1137/s0895479897326432

Hansen, P. C. (1992). Numerical tools for analysis and solution of Fredholm integral equations of the first kind. *Inverse problems*, *8*(6), 849. https://doi.org/10.1088/0266-5611/8/6/005

Hansen, P. C. (2007). Regularization tools version 4.0 for Matlab 7.3. *Numerical algorithms*, *46*(2), 189-194. https://doi.org/10.1007/s11075-007-9136-9

Kabanikhin, S. I. (2008). Definitions and examples of inverse and ill-posed problems. *Journal of Inverse and Ill-Posed Problems* 16, 317:357. https://doi.org/10.1515/jiip.2008.019

Li, H., Dong, L., Zhang, L., Yang, J. N., Gillin, M. T., & Zhu, X. R. (2011). Toward a better understanding of the gamma index: Investigation of parameters with a surface-based distance method. *Medical physics*, *38*(12), 6730-6741. https://doi.org/10.1118/1.3659707

Low, D. A., Harms, W. B., Mutic, S., & Purdy, J. A. (1998). A technique for the quantitative evaluation of dose distributions. *Medical physics*, *25*(5), 656-661. https://doi.org/10.1118/1.598248

OncologyMedPhys, (2019). Imrt quality assurance. Retrieved August 5, 2021 from https://oncologymedicalphysics.com/imrt-quality-assurance/

Renner, F., Schwab, A., Kapsch, R. P., Makowski, C., & Jannek, D. (2014). An approach to an accurate determination of the energy spectrum of high-energy electron beams using magnetic spectrometry. *Journal of Instrumentation*, *9*(03), P03004. https://doi.org/10.1088/1748-0221/9/03/p03004

Rogers, D. W. O., Faddegon, B. A., Ding, G. X., Ma, C. M., We, J., & Mackie, T. R. (1995). BEAM: a Monte Carlo code to simulate radiotherapy treatment units. *Medical physics*, *22*(5), 503-524. https://doi.org/10.1118/1.597552

Rustgi, S. N., & Rodgers, J. E. (1987). Analysis of the bremsstrahlung component in 6–18 MeV electron beams. *Medical physics*, *14*(5), 884-888. https://doi.org/10.1118/1.596018

Salvat, F., Fernández-Varea, J. M., & Sempau, J. (2021, August 5). PENELOPE-2008: a code system for Monte Carlo simulation of electron and photon transport (Issy-les-Moulineaux. France: OECD Nuclear Energy Agency.

Silva Neto, A. J., & Cella, N. (2006). A regularized solution with weighted Bregman distances for the inverse problem of photoacoustic spectroscopy. *Computational & Applied Mathematics*, *25*, 139-165. https://doi.org/10.1590/S0101-82052006000200003

Schanze, T. (2006). An exact D-dimensional Tsallis random number generator for generalized simulated annealing. *Computer physics communications*, *175*(11-12), 708-712. https://doi.org/10.1016/j.cpc.2006.07.012

Tikhonov, A. N. (1963). On the solution of ill-posed problems and the method of regularization. In Doklady Akademii Nauk, 151(3), 501-504.

Toutaoui, A., Khelassi-Toutaoui, N., Brahimi, Z., & Chami, A. C. (2009). Effects of energy spectrum on dose distribution calculations for high energy electron beams. *Journal of Medical Physics/Association of Medical Physicists of India*, *34*(1), 4. https://doi.org/10.4103/0971-6203.48715

Wilches-Visbal, J. H., & Da Costa, M. A (2019a). Algoritmo de recocido simulado generalizado para Matlab. *Ingeniería y Ciencia*, *15*(30), 117-140. https://doi.org/10.17230/ingciencia.15.30.6

Wilches-Visbal, J. H., & Da Costa, M. A (2019b). Inverse reconstruction of energy spectra of clinical electron beams using the generalized simulated annealing method. *Radiation Physics and Chemistry*, *162*, 31-38. https://doi.org/10.1016/j.radphyschem.2019.04.022

Wei, J., Sandison, G. A., & Chvetsov, A. V. (2006). Reconstruction of electron spectra from depth doses with adaptive regularization. *Medical physics*, *33*(2), 354-359. https://doi.org/10.1118/1.2161404

Wilches, J. H., Apaza, D. G., & Costa, A. M. D. (2020). Sobre la posibilidad de usar el metodo de regularizacion de tikhonov para reconstruir el espectro de energia de un haz clinico de electrones. *Momento*, (60), 1-17. https://doi.org/10.15446/mo.n60.75527

Xiang, Y., & Gong, X. G. (2000). Efficiency of generalized simulated annealing. *Physical Review E*, *62*(3), 4473. https://doi.org/10.1103/PhysRevE.62.447

Xu, Y., Pei, Y., & Dong, F. (2016). An adaptive Tikhonov regularization parameter choice method for electrical resistance tomography. *Flow Measurement and Instrumentation*, *50*, 1-12. https://doi.org/10.1016/j.flowmeasinst.2016.05.004

Zhengming, L., & Jette, D. (1999). On the possibility of determining an effective energy spectrum of clinical electron beams from percentage depth dose (PDD) data of broad beams. *Physics in Medicine & Biology*, *44*(8), N177. https://doi.org/10.1088/0031-9155/44/8/401

Zhu, T. C., Das, I. J., & Bjärngard, B. E. (2001). Characteristics of bremsstrahlung in electron beams. *Medical physics*, *28*(7), 1352-1358. https://doi.org/10.1118/1.1382608